TSUNAMI VULNERABILITY OF CRITICAL INFRASTRUCTURE: DEVELOPMENT OF FUNCTIONS FOR IMPACT ASSESSMENT

J. H. Williams[1], T. M. Wilson[2], L. Wotherspoon[3], N. Horspool[4], R. Paulik[5], E. M. Lane[6], M.W. Hughes[7]

[1] *PhD Candidate, School of Earth and Environment, University of Canterbury, james.williams@pg.canterbury.ac.nz*
[2] *Professor, School of Earth and Environment, University of Canterbury, thomas.wilson@canterbury.ac.nz*
[3] *Associate Professor, Civil and Environmental Engineering, University of Auckland, l.wotherspoon@auckland.ac.nz*
[4] *Natural Hazard Risk Scientist, Society and Infrastructure Department, GNS Science, n.horspool@gns.cri.nz*
[5] *Hazards Analyst, National Institute of Water and Atmospheric Research (NIWA), ryan.paulik@niwa.co.nz*
[6] *Hydrodynamics Scientist, National Institute of Water and Atmospheric Research (NIWA), emily.lane@niwa.co.nz*
[7] *Senior Lecturer, Department of Civil and Natural Resources Engineering, University of Canterbury, matthew.hughes@canterbury.ac.nz*

Abstract

Tsunami events over the last century have highlighted the potential for impacts on the built environment. Recent international tsunami events have provided an opportunity for the collection of post-event survey data for tsunami impacted critical infrastructure systems and networks. International research in the tsunami impacts domain has largely focused on direct building damage and casualty estimations, while only limited attention has been given to the impacts on critical infrastructure. New Zealand is a tectonically active country with substantial amounts of coastal infrastructure exposed to local, regional and distal source tsunamis. To effectively manage tsunami risk for New Zealand's critical infrastructure, including energy and transportation systems, the vulnerability of infrastructure networks and components must first be defined and assessed. This research develops empirical vulnerability functions for critical infrastructure components. These functions utilise post-event survey data from recent international tsunami events, including the 2011 Tohoku Tsunami, Japan, the 2015 Illapel Tsunami, Chile, and the 2018 Sulawesi Tsunami, Indonesia, which are adapted to the New Zealand context. A range of hazard intensity metrics (HIMs) and energy and transportation components are considered, as well as individual asset attributes relevant to assessing physical vulnerability, including construction design and material. These functions are applied in a risk assessment framework, using the impact and loss assessment tool RiskScape, and future work will estimate the costs and benefits of tsunami mitigation options for at risk critical infrastructure networks.

Keywords: tsunami; infrastructure; fragility function; tsunami impact; risk

1. Introduction

Tsunamis can damage and disrupt critical infrastructure, including energy, transportation, water and telecommunication networks, which are crucial to the everyday operation of society (e.g. habitability, accessibility, communication), as well as for efficient post-disaster response and recovery efforts [1]–[6]. Access to impacted populations, the provision of aid and repair works to other dependent lifelines are delayed by tsunami damage. It is also suggested that tsunami damage to infrastructure can account for up to 20% of the total economic cost of a tsunami disaster, mostly attributed to transport asset impacts [7]. Previous tsunami impact assessments have largely focused on direct building damage and casualty estimation, leaving a gap in the understanding of tsunami impacts on critical infrastructure [5], [6]. Given the importance of critical infrastructure to society, a prudent development for tsunami risk assessment is to develop suitable critical infrastructure impact assessment tools, specifically vulnerability models which provide a measure of loss (as either a potential for, or level of, damage) for a prescribed hazard intensity.

There are few comparable examples for tsunami damage to lifelines infrastructure (e.g. [5], [8]). Commonly used vulnerability metrics include fragility functions which are used to define the relationship between asset damage level and a hazard intensity (e.g. tsunami inundation depth; Koshimura et al., 2009). Fragility functions typically rely on relatively large samples of empirical or modelled impact data. Prior to recent tsunami events this type of quantitative data for infrastructure damages had not been collected.

The objectives of the current study are to (a) analyse post event tsunami survey data to develop a suite of tsunami fragility functions for infrastructure assets and to (b) apply these synthesised vulnerability metrics to a New Zealand-based tsunami impact, outage and recovery assessment. This study analyses infrastructure asset damage data from three recent tsunamis, the 2011 Tohoku Tsunami, Japan; the 2015 Illapel Tsunami, Chile; and the 2018 Sulawesi Tsunami, Indonesia. This study aims to address a gap in global knowledge of tsunami impacts on infrastructure to inform tsunami risk reduction. The data are collected and analysed considering a range of novel methods to overcome various challenges and to create consistent datasets for fragility function development. The following sections provide an analysis of data (Section 2) and the development of vulnerability functions (Section 3) followed by an impact assessment case study of Christchurch, New Zealand (Section 4) and then a summary of the study (Section 5). The study is currently biased toward the assessment of road vulnerability as these assets are often the most accessible and well preserved in terms of impacts following a tsunami event.

2. Methodology

2.1. Event 1: Tohoku Tsunami

The Tohoku Tsunami provided post-disaster survey teams with an extensive area from which to collect damage data on infrastructure assets. The data used for this analysis are the results of a comprehensive ground survey carried out in the days to weeks following the tsunami by the Japanese Government, City Bureau of the Ministry of Land, Infrastructure, Transport and Tourism (MLIT) [10]. The data relevant to this analysis included detailed road asset damage summaries and local maximum tsunami inundation depths for the exposed area within Miyagi and Iwate Prefectures, which were two of the regions most impacted [6], [8], [11], [12]. MLIT defined the length of affected roads and assigned each section a damage level (Table 1). The inundation depth and asset data, containing the damage observations, were requested by, and presented to, GNS Science as GIS shapefiles (.shp). Modelled maximum inundation depth (m) was available in 100 x 100 m grid cells, across the study area [6], [8], [11], [12].

Table 1: Damage classifications for roads, bridges, and utility poles [12], [13] and field examples of road damage levels from the 2015 Illapel Tsunami, Coquimbo, Chile, and equivalent bridge examples from the 2018 Sulawesi Tsunami, Indonesia (Modified from [6]).

| Damage Level	0	1	2	3
Damage State	No Damage	Minor	Moderate	Severe
Road Damage Description	*No damage*	*Minor damage to road surface. All lanes passable*	*Major damage to one lane. One lane impassable*	*Major damage to whole carriageway. All lanes impassable*
Road Image				
Bridge Damage Description	*No damage*	*Minor damage, often from impacts to the superstructure*	*Major damage to superstructure but still in place on piers. Superstructure may have been shifted*	*Complete washout of superstructure*
Bridge Image				
Utility Pole Damage Description	*No damage*	*Partial Damage, Repairable*	*Partial Damage, Unrepairable*	*Complete Damage*
Utility Pole Image				
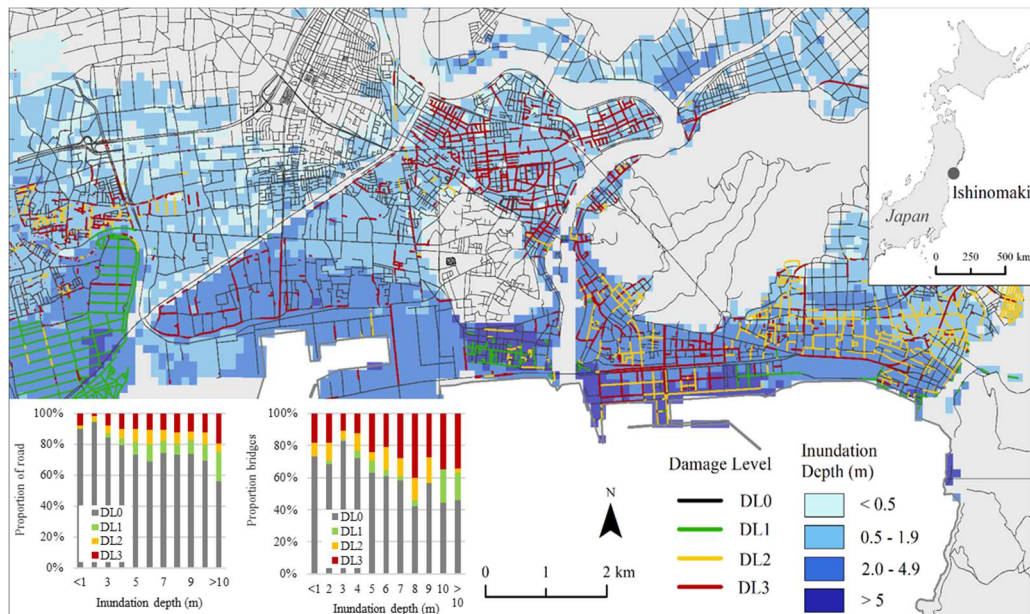
Figure 1: Road impacts in Ishinomaki, from the 2011 Tohoku Tsunami. Road-impact data modified from [12], [14]. Distributed under a Creative Commons BY-SA License. Graphs modified from [6].

3

The Tohoku dataset lacked spatial non-damaged asset data (DL0), which is crucial to defining proportional damage probabilities. Therefore, all roads and bridges within the inundation area were extracted from OpenStreetMap (OSM), (OpenStreetMap contributors, 2015) or were digitized from aerial imagery and those which were not recorded in the MLIT data were assumed undamaged (DL0). This resulted in a complete dataset of roads and bridges exposed to the tsunami, each with an observed damage level (DL0 – DL3). Figure 1 shows an example of observed damage levels for roads in the town of Ishinomaki within the study area. Tsunami inundation depths MLIT (2012) were then assigned to each road length and in the case of bridges, inundation depth was normalised to the height above the base of a bridge deck. The results of this analysis are presented in Section 3 as fragility functions.

Asset attribute information should ideally include road construction type, allowing for the development of construction specific fragility functions. As this was not included in the MLIT dataset [12], the closest equivalent was road-use type category based on jurisdiction (0; Unclassified, 1; State road, 2; Main local road, 3; General prefectural road, 4; Municipalities road, 5; Lowest class road). These classifications were then converted to road-use type equivalent categories (0; Unclassified, 1; Motorway, Trunk, Primary, 2; Secondary, 3; Residential, Road, 4; Tertiary, 5; Construction, Service, Unsurfaced) to ensure compatibility with OSM (OpenStreetMap contributors, 2015) data . Roads digitised from satellite imagery were assumed to be in class 3. However, those that could not be classified were 'Unclassified' (0) which have not contributed towards the resulting fragility functions. These road use classes link to different traffic loading levels, which inform road design, therefore these data broadly encompass differences in construction type, but some degree of overlap is assumed. Bridge construction materials were not available, neither was bridge deck base height above ground, both of which would be necessary for a higher resolution fragility function [8], [15].

Fragility functions that do not consider topography may not accurately represent tsunami damage characteristics when used for subsequent impact assessment. Therefore this study defines vulnerability for two broad coastal settings, 'coastal plains' and 'coastal valleys' (Figure 2), to develop specific vulnerability curves similarly to[16] and [17]. The resulting fragility functions are presented in Section 3.
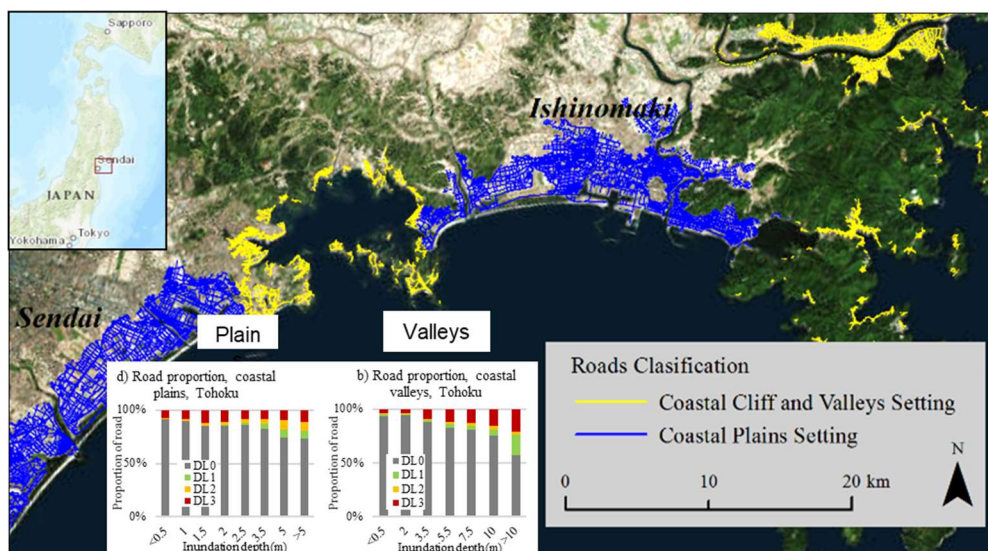

Figure 2: Coastal topographic settings for inundated roads for the 2011 Tohoku Tsunami. Note: all roads North of Ishinomaki are Coastal Valleys; all roads South of Sendai are Coastal Plains. Road data modified from [12] and [14]. Distributed under a Creative Commons BY-SA License. Japan topographic imagery sourced from [18], Tohoku regional satellite imagery sourced from [19]. Modified from [6].

2.2. Event 2: Illapel Tsunami

A census-style field survey was conducted in Coquimbo, Chile, between 8-12 days after the Illapel tsunami, at the invitation of the Chilean Association on Seismology and Earthquake Engineering (ACHISINA). The

4

team included members from GNS Science, National Institute of Water and Atmospheric Research (NIWA), Wellington Lifelines Group, Auckland City Council, University of Canterbury and was supported by Chilean researchers from University of Valparaiso [6]. Coquimbo was selected as the focus of the post-event survey as it was the region most impacted in this event and also represented a small enough study area to collect data in a short timeframe. Damage, asset and hazard data were collected, using the Real-time Individual Asset Collection Tool (RiACT; [20]) in accordance with International Tsunami Survey Team (ITST) procedures [21]. Asset damage was defined using a four-tier damage-level classification in accordance with the MLIT classification structure (Table 1). This was done to be consistent with the Tohoku dataset, which was already available and represented the largest damage repository of tsunami impacts on roads in particular. Although this classification of damage level could have been refined, the field team decided it still represented a relatively efficient method in-field and at a resolution high enough to incorporate the range of observed damage types. Most roads surveyed in the inundation area were founded on sandy material, with a compacted granular subbase and a thin asphalt surface (flexible pavement construction method; [22]). There were few 'both-lane' wash-outs, with minor / single lane wash-outs being more common, and many washouts occurred where a culvert ran beneath the road surface. Inundation depth was estimated in the field by measuring watermarks against vertical structures (e.g. buildings, utility poles). A total of 978 watermarks were recorded across the survey area which represented inundation depth above ground level. The total survey area included an approximately 7 km stretch of coastline [6].

Asset data collected included utility poles, roads, bridges, water pipes, hydrants, storm water drains, footpaths, gas tanks, electricity stations, pump stations and seawalls, although only roads are presented so far for this study. Roads were separated into approximately 50 m sections, and assigned the corresponding damage level (DL0-DL3) and inundation depth, through interpolation of the surveyed watermarks, at the centre of each feature using inundation depth bins of 0.25 m (0.0 - 0.25 m, 0.25 – 0.5 etc.). The total length of road (in km) for each depth bin and for each damage level was tabulated for each HIM by count and proportion (Figure 3, [6]). The resulting fragility functions are presented in Section 3.
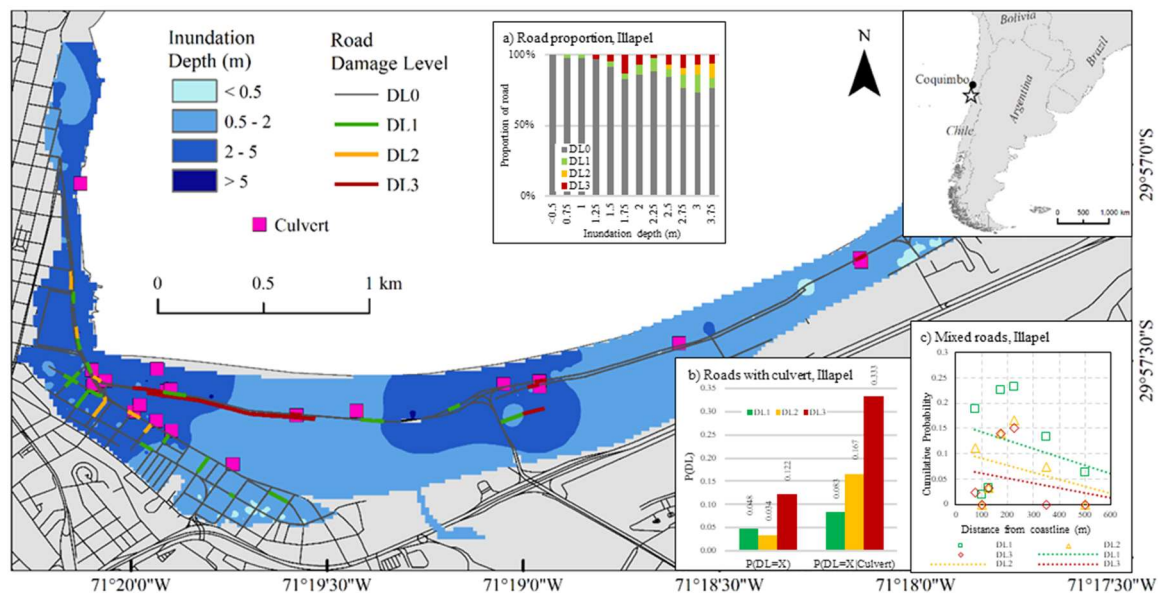

Figure 3: Road impacts in Coquimbo for the 2015 Illapel Tsunami, [14]. Distributed under a Creative Commons BY-SA License. Modified from [6].

While inundation depth has been used as the HIM, as outlined above, other potential metrics that might have a bearing on asset vulnerability were also considered. As mentioned above, road damage was observed at many culvert openings especially along the coastal esplanade (Figure 3). This damage is consistent with the principle of contraction scour [23], which occurs when the depth of inundation exceeds an opening and the inundation becomes contracted. The inundation is directed down and through the structure, causing an increase

5

in the velocity and shear stress around the outlet, therefore increasing scour [6]. Inundation speed, inundation depth, the degree of submersion and size of the culvert are all factors dictating contraction scour intensity. Scour can also be exacerbated by the enhanced turbulence and vortex formation in this inundation. Scour around culverts can also be caused by the back-inundation of receding water. Recorded culvert locations were used to assign the presence of a culvert/outfall pipe (present '1', not present '0') to each 50m section of road. The frequency and proportion of road sections with a culvert were tabulated for each damage level (Figure 3b). This analysis is not conducive with fragility functions, due to the limited number of culverts surveyed, so none are developed in this study. The associated road damage levels indicate a relationship between the presence of a culvert and an increased damage level. Furthermore, all instances of a culvert in this event resulted in road damage to some extent, and in most cases moderate or severe damage (DL 2 and DL3).

Tsunami inundation velocity is known to have a considerable influence on asset impacts, especially due to scour [5]. However, inundation velocity data were not available for the Illapel dataset, so distance from the coast is used as a proxy. This assumes a constant deterioration of landward wave energy including horizontal and vertical buoyancy pressure as a tsunami wave moves inland (from friction and gravity). This was observed for road assets in Coquimbo as damage levels reduced with distance from the coastline. A measure of distance from the coast was calculated at 25 m inundation distance bins (i.e. $0.0 – 25.0$ m, $25 – 50$ m etc.). Since distance from the coastline is not a direct damage causing process, the analysis not conducive with fragility functions, so none are developed for this study, however, there is a clear trend between higher probabilities of damage occurring closer to the coastline as expected (Figure 3c). This may be an indicator for deteriorating wave energy (due to surface friction and gravity) but could simply be an indicator of increased inundation depths at the coast since there is no empirical evidence of hydrodynamic forces in the Illapel event. The same was noted in a study of building vulnerability in the Illapel event [24], particularly with lower damage occurring beyond a wetland area in Coquimbo and behind a raised railway ballast, when compared to those nearer the coast.

Tsunami generated debris can cause considerable disruption to infrastructure, including transportation networks, through direct damage and through blocking routes. Therefore the effects of debris on an asset's level of service is considered, and a new HIM (distance from the landward inundation extent) is used. To assess the relationship between debris and a roads level of service in Coquimbo, debris distribution data is required. However debris clean-up had begun prior to the survey, so publicly available drone mounted camera footage [25] was used to map out debris density on roadways. These were classified into five service levels (SL), as defined in Table 2. SLU represents areas of ponding observed and is classed separately since the depth and amount of debris entrained is not known. If there was no debris, a road was assigned SL0. To account for potential horizontal sorting of debris, the distance from tsunami inundation extent (i.e. the greatest recorded landward observations of tsunami inundation) was used and each road was assigned an associated value. The local sea port, of which are typically well-defined regions of debris origin [26], was located along the South-West to North-West inundated coastline. As well as inundation depth (in m) and distance from the coast (m), each road section was now assigned a distance from the inundation extent value (m) and a level of service (SL0 - SL3 or SLU), (Figure 4). For each distance measure, road length frequency was tabulated into 25 m bins (i.e. $0.0 – 25.0$ m, $25.0 – 50$ m etc.), for each service level. There is higher debris density between approximately $75.0 – 150.0$ m ($11 – 22\%$) from in-land inundation extent (Figure 4a). Debris density probability is consistently lower, for all levels of service, between $0.0 – 75.0$ m ($0 – 11\%$) from in-land inundation extent and $200.0 – 672$ m ($30 – 100\%$) from in-land inundation extent. SL1 has a much higher probability of occurrence than SL2 and SL3 at distances > 200 m from in-land inundation extent (Figure 4a). This is consistent with field observations where debris is consistently distributed across an inundation area during landward and seaward inundations. There was no such empirical source of debris density observations available for the 2011 Tohoku Tsunami, so this is not considered in the analysis of the Tohoku dataset.

6

Table 2: Classification schema for road service level for the 2015 Illapel Tsunami, modified from [6]. Images taken as screenshots sourced from [25].

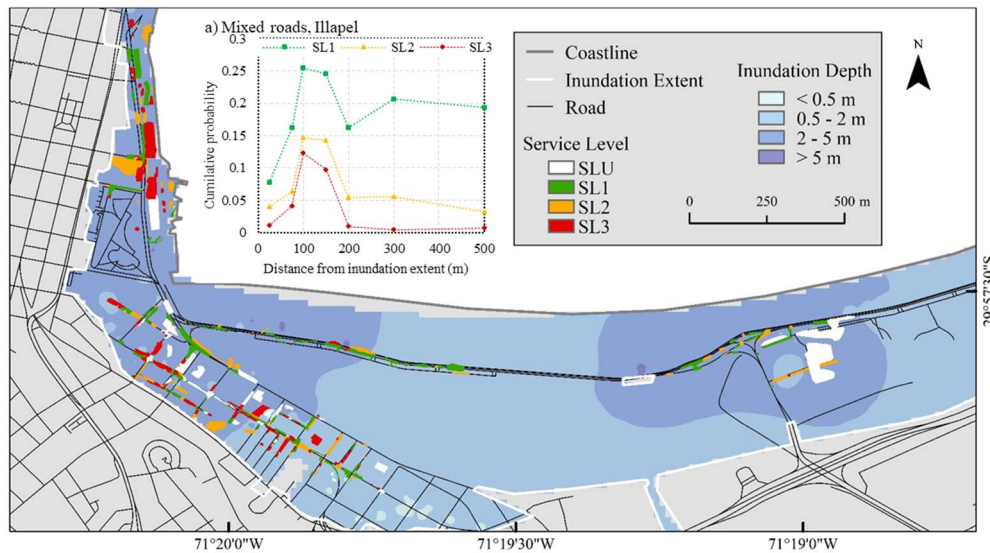| Service Level	U	0	1	2	3
Service Level Description	Unknown (surface ponding)	No loss of service	Vehicle access at a reduced speed	All-wheel drive vehicle access at reduced speed	No vehicle access
Image		-			

Figure 4: Service levels associated with debris on roads in Coquimbo for the 2015 Illapel Tsunami,[14]. Distributed under a Creative Commons BY-SA License. Modified from [6].

2.3. Event 3: Sulawesi Tsunami

The survey team collected tsunami flow depth and damage information in Palu City in accordance with post-tsunami survey procedures [21]. Survey observations and data collection were implemented using the Real Time Asset Capture Tool (RiACT; [20]). Spatial information collected for lifelines infrastructure included the GPS coordinates, damage length, damage width and the surveyed variables and attributes [13]. Additionally, the data collection in Palu City included surveyed impacts for each exposed asset. Survey area reconnaissance identified roads and utility poles as most frequently exposed to tsunamis and accessible for onsite damage observations. Observed damage levels were categorised using the four-tier damage schema (Table 1). The approach enabled consistent database development, ensuring comparability with other tsunami damage datasets (e.g. Tohoku and Illapel).

Paulik et al, 2019, [13] collected tsunami flow depths and empirical tsunami damage data on buildings, roads and utility poles in Palu City. As is often the case with post-event field surveys, some aspects of the exposed assets were not possible to record in-field. This included exposed, but undamaged, assets toward the inland inundation extent of the tsunami and assets at the highest level of impact which were completely washed away. This is due to the perishable nature of post-event hazard indicators and impact damage which, in the case of Palu, was either weathered (watermarks) or quickly cleaned up (damaged assets and objects with

7

watermarks). This made tracing the exact extent of inundation difficult and observing washed away assets unlikely. Due to these limitations, the field observations are therefore supplemented with remotely sensed observations. Using online tools including Google Earth 'street view'[27] and the pre-event imagery for Palu City which was captured in September 2018 , within weeks of the Sulawesi Earthquake and Tsunami. This imagery was used to check each utility pole and road segment against the field data. This process captured missing assets, confirmed asset attributes, such as construction type and material, and completed the dataset up to the landward inundation extent. In the instance of a missing utility pole or road from the field survey data, this was added remotely and assumed to be in DL3. All assets up to the inundation run-up extent were inspected digitally and assumed to be in DL0 if not already included in the survey data. For roads, the spatial point data were digitised as a series of lines to represent the spatial length of each damage observation, including DL0. This allowed for road geometry (i.e. length) to be calculated remotely.

Using the 397 watermarks collected by Paulik et al, 2019, [13] an interpolation was made and each asset assigned a corresponding inundation depth. At this point all road and utility pole assets within the inundation extent were now captured spatially in the data, each with an assigned damage level and HIM (Figure 5). The resulting fragility functions are presented in Section 3.
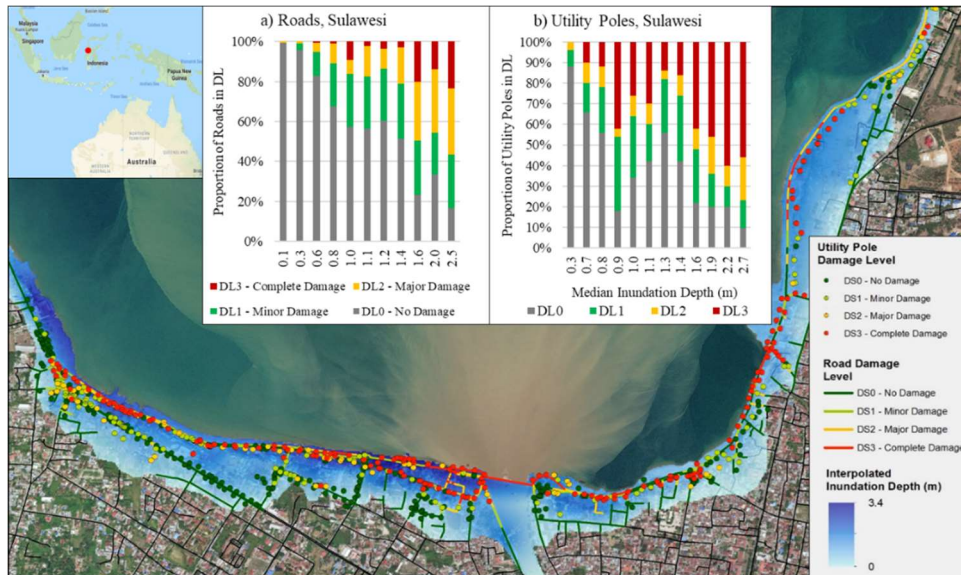

Figure 5: Roads and utility poles impacts for the 2018 Sulawesi Tsunami, modified from [6], [13].

3. Developing Fragility Functions

The asset damage probabilities for each damage level were calculated and shown against a median value within increasing HIM bins, to account for lower amounts of data at higher HIM. Following the methods of Koshimura et al., 2009, [9] linear regression analysis was performed to develop the normal (Log-normal) cumulative distribution function vulnerability curves. A probability P of reaching or exceeding a damage level for a given hazard intensity value is given by either Eq. (1) or (2):

$$P(x) = \Phi \left[\frac{x - \mu}{\sigma} \right] \tag{1}$$

$$P(x) = \Phi \left[\frac{\ln x - \mu\prime}{\sigma\prime} \right] \tag{2}$$

where Φ is the standardized normal (lognormal) distribution function, x is the HIM (i.e. inundation depth), μ and σ ($\mu\prime$ and $\sigma\prime$) are the mean and standard deviation of x (ln x) respectively. Two statistical parameters of fragility function, i.e. μ and σ ($\mu\prime$ and $\sigma\prime$), are obtained by plotting x (ln x) and the inverse of Φ^{-1} on normal or lognormal plots, and performing the linear least-squares fitting of this plot. Two parameters are obtained by

8

taking the intercept (= μ or μ′) and the slope (= σ or σ′) in either Equation (3) or (4), depending on the result of the least-squares fitting:

$$x = \sigma\Phi^{-1} + \mu \tag{3}$$

$$\ln x = \sigma'\Phi^{-1} + \mu' \tag{4}$$

The resulting fragility functions from each dataset are presented in Figure 6. As this is an ongoing study only a limited number of functions are presented. The fragility functions in Figure 7 then present an example of refined curves for Tohoku roads (i.e. data from Figure 6a) which also consider use-type category and topographic setting as outlined above in Sub-section 2.1.
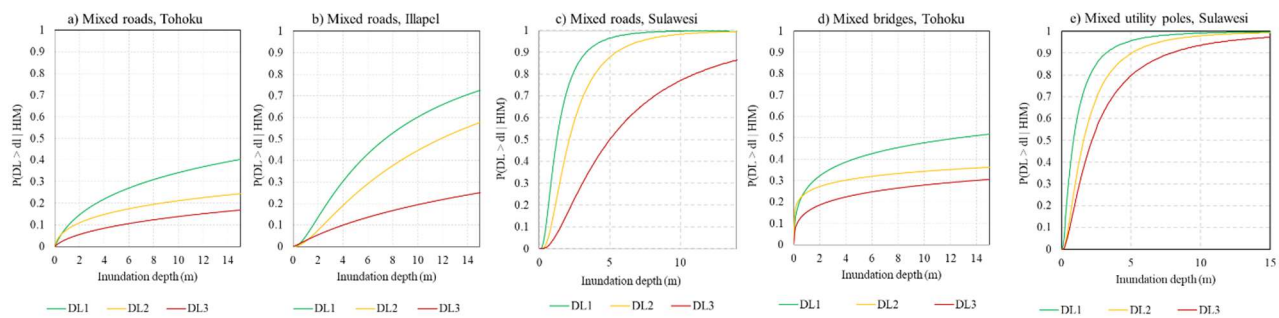

Figure 6: Fragility functions for mixed construction road, bridge, and utility pole assets. Modified from [6].
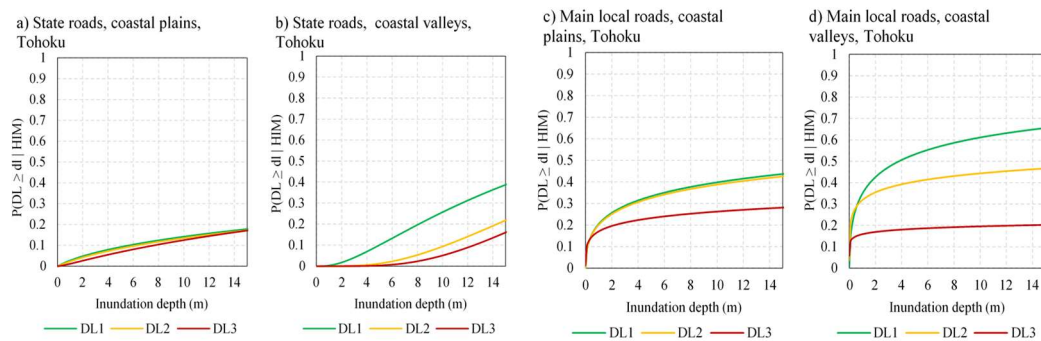

Figure 7: Fragility functions for Tohoku roads considering use-type and topographic setting. Modified from [6].

4. Case Study Application

The synthesised fragility functions are applied to a deterministic tsunami impact assessment process for infrastructure assets in Christchurch, New Zealand. Christchurch is located on New Zealand's east coast on the western edge of the Pacific. The tsunami hazard for Christchurch is estimated to be > 9.5 m and > 12.5 m wave heights at the coast at the 50th and 84th percentiles, respectively, for a 2500 year return interval, with the most likely tsunami source for both a 2500- and 500-year event at the 50th percentile being the Peru subduction zone [5], [28], [29]. The impact assessment was carried out using the impact and loss assessment tool RiskScape 2.0 and utilises the synthesised fragility functions for roads, which consider construction standards and topographic setting (Figure 7), and for utility poles (Figure 6e). The tsunami model used is based on a Mw 9.485 Peru subduction zone earthquake source for 2018 sea levels [30]. The initial results of this impact assessment are presented in Figure 8.
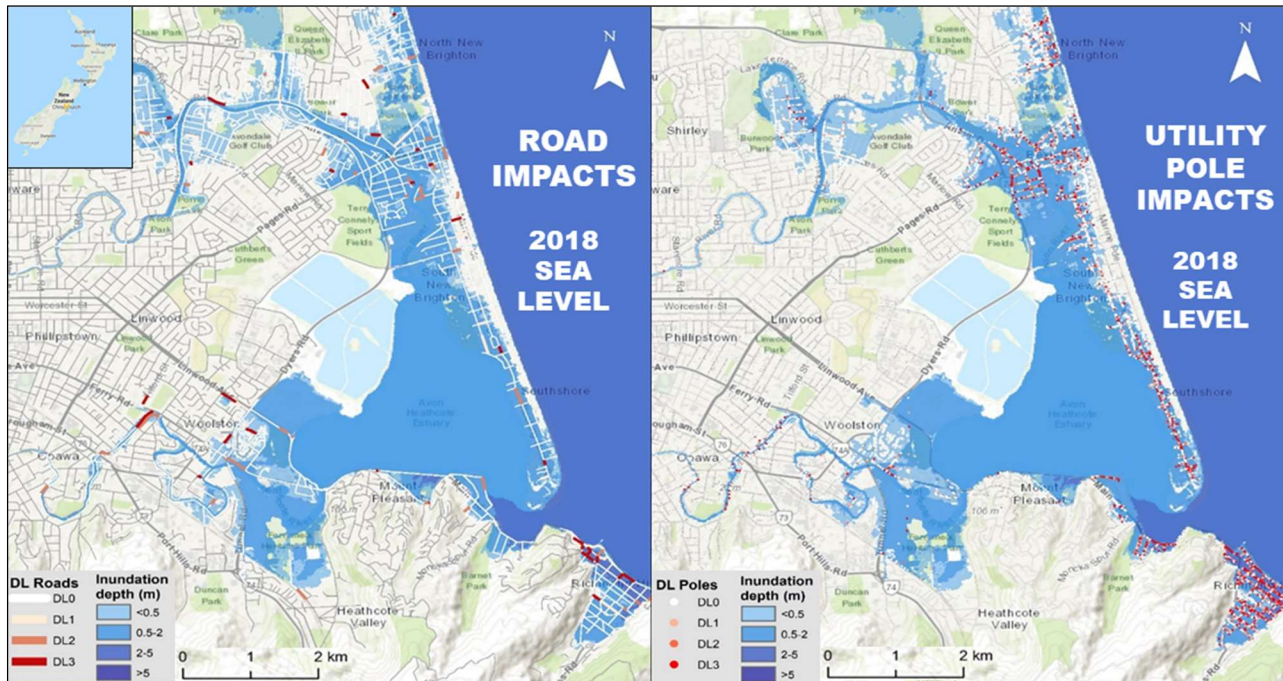
9

Figure 8: Results of impact assessment for Christchurch, New Zealand, utility poles and roads for an equivalent Mw 9.485 Peru subduction zone tsunami model sourced from [30], Christchurch imagery sourced from [18].

Using similar methodology to the Wellington Resilience Project Business Case [31] for a Wellington Fault earthquake, a model will be developed for direct (e.g. asset damage, Figure 8) and indirect (e.g. loss of network connectivity) losses resulting from tsunami impacts on infrastructure lifelines. The direct impacts will be modelled following the impact assessment framework by Williams, 2016, [29] while loss of service and outage time modelling will be developed in collaboration with local infrastructure operators and informed by case studies of previous tsunami events as is done by Wellington Lifelines, 2019, [31].

5. Summary

This paper has presented an ongoing study on tsunami impacts on infrastructure. Empirical post-event field survey data from three recent damaging international tsunami events are used to develop fragility functions. An example of ongoing work to refine fragility functions for a range of hazard, asset and topographic parameters is also presented, representing road fragility for the 2011 Tohoku tsunami which consider use-type and topographic setting for the probability of reaching or exceeding a given damage level. The synthesised fragility functions are applied through an impact assessment case-study of roads and electricity distribution utility poles for Christchurch, New Zealand. Continued research will include the development and application of fragility functions from future tsunami events and for more infrastructure assets. Subsequent impact assessments will also incorporate the results of analyses on further impact observations such as culvert damage, and debris-based service level as presented in this paper. A framework for assessing lifeline outage and recovery times is also in development which will involve the input of local lifeline utility operators and managers.

7. References

[1]   D. M. Frangopol and P. Bocchini, "Bridge network performance, maintenance and optimisation under uncertainty: accomplishments and challenges," *Struct. Infrastruct. Eng. Maintenance, Manag. Life-Cycle Des. Perform.*, vol. 8, no. 4, pp. 341–356, 2012.

[2]   H. Nakanishi, J. Black, and K. Matsuo, "Disaster resilience in transportation: Japan earthquake and

10

tsunami 2011," *Int. J. Disaster Resil. Built Environ.*, vol. 5, no. 4, pp. 341–361, 2014.

[3]   M. Saatcioglu, "Performance of Structures Affected by the 2004 Sumatra Tsunami in Thailand and Indonesia," in *The Indian Ocean Tsunami: Balkema-proceedings and monographs in engineering, water and earth sciences*, T. S. Murty, U. Aswathanarayana, and N. Nirupama, Eds. London, UK: Taylor & Francis, 2007, pp. 297–321.

[4]   J. Birkmann *et al.*, "Extreme Events, Critical Infrastructures, Human Vulnerability and Strategic Planning: Emerging Research Issues," *J. Extrem. Events*, vol. 03, no. 04, p. 1650017, 2016.

[5]   J. H. Williams *et al.*, "Tsunami impact assessment: development of vulnerability matrix for critical infrastructure and application to Christchurch, New Zealand," *Nat. Hazards*, vol. submitted, no. 0123456789, pp. 1–28, Apr. 2019.

[6]   J. H. Williams *et al.*, "Assessing Transportation Vulnerability to Tsunamis : Utilising Post- event Field Data from the 2011 Tohoku Tsunami , Japan , and the 2015 Illapel Tsunami , Chile," no. October, 2019.

[7]   M. Marchand, J. Buurman, A. Pribadi, and A. Kurniawan, "Damage and casualties modelling as part of a vulnerability assessment for tsunami hazards: a case study from Aceh, Indonesia," *J. Flood Risk Manag.*, vol. 2, no. 2, pp. 120–131, 2009.

[8]   N. A. Horspool and S. Fraser, "An Analysis of Tsunami Impacts to Lifelines," *GNS Sci. Consult. Rep. 2016/22*, 2016.

[9]   S. Koshimura, Y. Namegaya, and H. Yanagisawa, "Tsunami fragility: a new measure to identify tsunami damage," *J. Disaster Res.*, vol. 4, no. 6, pp. 479–488, 2009.

[10]   MLIT, "MLIT," 2013. [Online]. Available: http://www.mlit.go.jp/en/index.html. [Accessed: 12-Dec-2015].

[11]   R. T. Eguchi, M. T. Eguchi, J. Bouabid, S. Koshimura, and W. P. Graf, "HAZUS Tsunami Benchmarking, Validation and Calibration," 2013.

[12]   MLIT, "Archive of the Great East Japan Earthquake Tsunami disaster urban reconstruction assistance survey.," 2012. [Online]. Available: http://fukkou.csis.u-tokyo.ac.jp/. [Accessed: 01-Jun-2015].

[13]   R. Paulik *et al.*, "Tsunami Hazard and Built Environment Damage Observations from Palu City after the September 28 2018 Sulawesi Earthquake and Tsunami," *Pure Appl. Geophys.*, 2019.

[14]   OpenStreetMap contributors, "Open Street Map," 2015. [Online]. Available: https://www.openstreetmap.org. [Accessed: 15-Oct-2015].

[15]   G. Shoji and T. Moriyama, "Evaluation of the Structural Fragility of a Bridge Structure Subjected to a Tsunami Wave Load," *J. Nat. Disaster Sci.*, vol. 29, no. 2, pp. 73–81, 2007.

[16]   R. De Risi, K. Goda, T. Yasuda, and N. Mori, "Is flow velocity important in tsunami empirical fragility modeling?," *Earth-Science Rev.*, vol. 166, pp. 64–82, 2017.

[17]   A. Suppasri *et al.*, "Building damage characteristics based on surveyed data and fragility curves of the 2011 Great East Japan tsunami," *Nat. Hazards*, vol. 66, no. 2, pp. 319–341, 2013.

[18]   ESRI contributors, "'Topographic' [basemap]. Scale Not Given," 2019. [Online]. Available: https://www.arcgis.com/home/item.html?id=30e5fe3149c34df1ba922e6f5bbf808f. [Accessed: 12-Aug-2019].

[19]   ESRI contributors, "'World Imagery' [basemap]. Scale Not Given," *"World Imagery,"* 2019. [Online]. Available: https://www.arcgis.com/home/item.html?id=10df2279f9684e4a9f6a7f08febac2a9. [Accessed: 12-Aug-2019].

[20]   S.-L. Lin, A. King, N. Horspool, V. Sadashiva, R. Paulik, and S. Williams, "Development and Application of the Real-Time Individual Asset Attribute Collection Tool," *Front. Built Environ.*, vol.

11

5, no. February, pp. 1–14, Feb. 2019.

[21] D. Dominey-Howes *et al.*, "International Tsunami Survey Team (ITST) Post-Tsunami Survey Field Guide," vol. 2, 2012.

[22] D. W. and J. C. N. M E Nunn, A Brown, "Design of long-life flexible pavements for heavy traffic Prepared for Highways Agency , British Aggregate Construction," *Transp. Res. Lab.*, vol. TRL REPORT, no. June, 1997.

[23] B. M. Duc and W. Rodi, "Numerical Simulation of Contraction Scour in an Open Laboratory Channel," *J. Hydraul. Eng.*, vol. 134, no. 4, pp. 367–377, 2008.

[24] R. Aránguiz, L. Urra, R. Okuwaki, and Y. Yagi, "Development and application of a tsunami fragility curve of the 2015 tsunami in Coquimbo, Chile," *Nat. Hazards Earth Syst. Sci.*, vol. 18, no. 8, pp. 2143–2160, 2018.

[25] Puerto Creativo, "Coquimbo y Tongoy Terremoto Tsunami Earthquake Drone," 2015. [Online]. Available: https://www.youtube.com/watch?v=B7mH8BV6RWQ.

[26] C. Naito, C. Cercone, S.M.ASCE, H. R. Riggs, S.M.ASCE, and D. Cox, "Procedure for Site Assessment of the Potential for Tsunami Debris Impact," *J. Waterw. Port, Coastal, Ocean Eng.*, vol. 140, no. 2, pp. 223–232, 2014.

[27] Google, "Google Earth Pro Desktop." 2015.

[28] W. L. Power, "Review of Tsunami Hazard in New Zealand (2013 Update)," *GNS Sci. Consult. Rep. 2013/131*, 2013.

[29] J. H. Williams, "Impact assessment of a far-field tsunami scenario on Christchurch City infrastructure.," 2016.

[30] E. M. Lane, A. Kohout, J. Sykes, J. Arnold, J. Bind, and S. Williams, "Distant tsunami inundation modelling incorporating dune failures and river flow in Christchurch," 2017.

[31] Wellington Lifelines, "REGIONAL RESILIENCE PROJECT WELLINGTON LIFELINES PROJECT Protecting Wellington ' s Economy Through Accelerated Infrastructure Investment Programme Business Case," 2019.

12